LETTER

doi:10.1038/nature09535

Stage-specific sensitivity to p53 restoration during lung cancer progression

David M. Feldser[1], Kamena K. Kostova[1], Monte M. Winslow[1], Sarah E. Taylor[1], Chris Cashman[1], Charles A. Whittaker[1], Francisco J. Sanchez-Rivera[1], Rebecca Resnick[1], Roderick Bronson[2], Michael T. Hemann[1] & Tyler Jacks[1]

Tumorigenesis is a multistep process that results from the sequential accumulation of mutations in key oncogene and tumour suppressor pathways. Personalized cancer therapy that is based on targeting these underlying genetic abnormalities presupposes that sustained inactivation of tumour suppressors and activation of oncogenes is essential in advanced cancers. Mutations in the p53 tumour-suppressor pathway are common in human cancer and significant efforts towards pharmaceutical reactivation of defective p53 pathways are underway[1–3]. Here we show that restoration of p53 in established murine lung tumours leads to significant but incomplete tumour cell loss specifically in malignant adenocarcinomas, but not in adenomas. We define amplification of MAPK signalling as a critical determinant of malignant progression and also a stimulator of Arf tumour-suppressor expression. The response to p53 restoration in this context is critically dependent on the expression of Arf. We propose that p53 not only limits malignant progression by suppressing the acquisition of alterations that lead to tumour progression, but also, in the context of p53 restoration, responds to increased oncogenic signalling to mediate tumour regression. Our observations also underscore that the p53 pathway is not engaged by low levels of oncogene activity that are sufficient for early stages of lung tumour development. These data suggest that restoration of pathways important in tumour progression, as opposed to initiation, may lead to incomplete tumour regression due to the stage-heterogeneity of tumour cell populations.

Experimental restoration of p53 (also known as *Trp53*) tumour-suppressor function has highlighted the potential for therapeutic intervention of this pathway to treat cancer and has uncovered a diversity of anti-tumour responses in different tumour types[4–6]. These studies imply that some types of cancer rely upon sustained inactivation of the p53 pathway as these tumours undergo rapid, and sometimes complete, regression once p53 is restored. To elucidate the role of p53 in lung cancer progression and to evaluate the therapeutic potential of p53 reactivation in this disease, we analysed the effect of *Trp53* restoration in a mouse model of $Kras^{G12D}$-driven lung cancer at different time points in tumour progression. *Trp53* restoration was achieved by delivering tamoxifen to 4-week-old $Kras^{LA2/+};Trp53^{LSL/LSL};Rosa26^{CreERT2}$ mice (Supplementary Fig. 1). We measured tumour volumes with micro-computed tomography and tumour areas by histological analysis. Surprisingly, at this time point, *Trp53* restoration did not significantly change tumour size or number (Fig. 1a, b). Efficient deletion of the '*STOP*' element from $Trp53^{LSL}$ alleles was evident in all tumours analysed (Supplementary Fig. 2).

To establish the timing and stage of tumour progression when the effects of p53 mutation are evident, we compared $Kras^{LA2/+};Trp53^{LSL/LSL}$ tumours to tumours from age-matched $Kras^{LA2/+};Trp53^{+/+}$ mice. At four weeks, most tumours were adenomatous hyperplasias or alveolar adenomas with monomorphous epithelial cells and uniform nuclei (Supplementary Fig. 3). In $Kras^{LA2/+};Trp53^{LSL/LSL}$ mice at this age, a small fraction of tumours had mixed histological features with focal areas of adenocarcinoma within lower grade lesions (Fig. 1c). Although most tumours in $Kras^{LA2/+};Trp53^{+/+}$ and $Kras^{LA2/+};Trp53^{LSL/LSL}$ mice were of similar grade, the presence of pleomorphic nuclei was a prominent feature of $Kras^{LA2/+};Trp53^{LSL/LSL}$ tumours compared to $Kras^{LA2/+};Trp53^{+/+}$ tumours (Fig. 1d). This observation may indicate

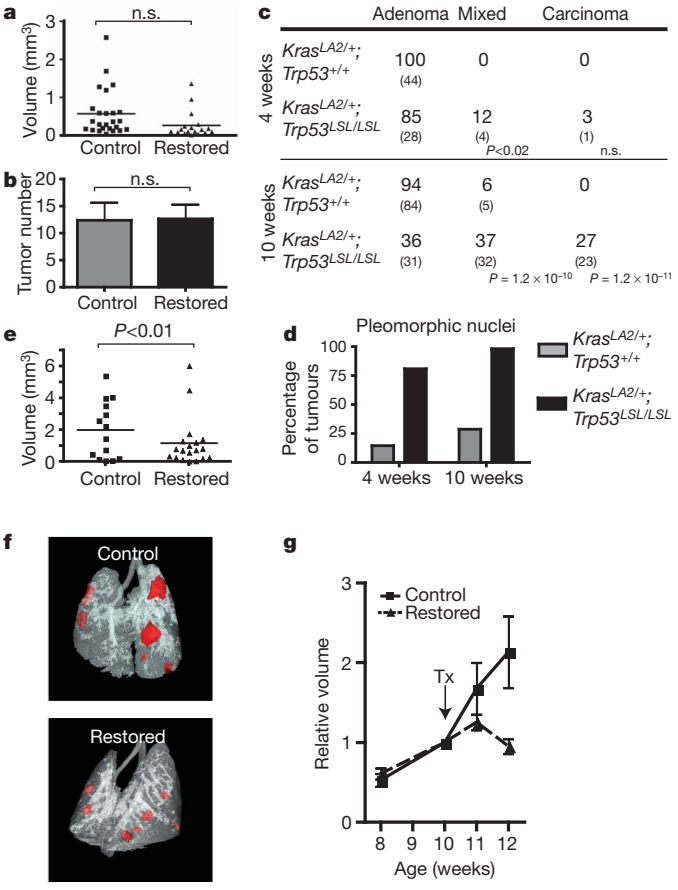

Figure 1 | Lung adenomas are apathetic to *Trp53* restoration, whereas adenocarcinomas are responsive. **a**, Individual tumour volumes were determined by micro-computed tomography 2 weeks after *Trp53*-restoration that began at 4 weeks of age. **b**, Histological sections were evaluated for tumour number in control ($n = 10$) and restored ($n = 12$) mice. **c**, Tumour number and grade at 4 and 10 weeks of age. Individual tumours from $Kras^{LA2/+};Trp53^{LSL/LSL}$ ($n = 5$) and $Kras^{LA2/+};Trp53^{+/+}$ ($n = 4$) mice. The percentage and number (in parentheses) of tumours is indicated. **d**, Pleomorphic nuclei in tumour samples from **c** (see also Supplementary Fig. 5). **e**, Restoration of *Trp53* in 10-week-old animals results in significantly diminished tumour size. Tumour volumes determined by micro-computed tomography 2 weeks after p53 restoration. **f**, Representative tomograms from micro-computed tomography analysis at 12 weeks. **g**, Serial micro-computed tomography analysis of individual tumours. Average relative size of tumours is plotted, error bars represent s.e.m. n.s., not significant; Tx, treatment.

[1]Koch Institute for Integrative Cancer Research, Department of Biology, and Howard Hughes Medical Institute, Massachusetts Institute of Technology, 77 Massachusetts Avenue, Cambridge, Massachusetts 02139, USA. [2]Tufts University, and Harvard Medical School, 77 Avenue Louis Pasteur, Boston, Massachusetts 02115, USA.

that $Kras^{LA2/+};Trp53^{LSL/LSL}$ tumour cells have a higher degree of genetic instability that may facilitate tumour progression at a later time point.

At 10 weeks of age, $Kras^{LA2/+};Trp53^{LSL/LSL}$ tumours were much more likely to exhibit nuclear pleomorphism and regions of advanced histopathology. Beyond these mixed grade tumours, frank adenocarcinomas were present exclusively in $Kras^{LA2/+};Trp53^{LSL/LSL}$ mice (Fig. 1c). Given that high-grade tumours were more prevalent in older mice, we restored *Trp53* in 10-week-old $Kras^{LA2/+};Trp53^{LSL/LSL};Rosa26^{CreERT2}$ mice. Here, restoration of *Trp53* resulted in significantly smaller tumours compared to controls after 2 weeks (Fig. 1e, f). To monitor the response of individual tumours, we performed serial micro-computed tomography before and after *Trp53* restoration. Although control tumours continued to grow during the 2-week time course, we found that the average size of tumours after *Trp53* restoration was static (Fig. 1g). However, the response of individual tumours was variable (Supplementary Fig. 4). Thus, we proposed that only a subset of tumours is sensitive to *Trp53* restoration.

Upon *Trp53* restoration, adenocarcinomas, but not adenomas, displayed multiple features of cellular senescence. Both p53 and the p53 target gene *Cdkn1a* (also known as p21) were detectable in tumours as early as 3 days after restoration, but were specifically confined to tumours with adenocarcinomatous features (Fig. 2b and Supplementary Fig. 5). In addition to observing p21 induction in the adenocarcinomas of 10-week-old mice (Fig. 2c), p21 was also induced in the few carcinomas found in the 4-week-old animals (data not shown). Moreover, *Trp53* restoration caused reduced cellular proliferation (Fig. 2d). Of note, the percentage of tumours with adenocarcinomatous features was significantly diminished 2 weeks after *Trp53* restoration with many tumours showing gaps between collections of low-grade tumour cells filled with foam macrophages (Fig. 2a, e). Despite this evidence of cell loss, we failed to find signs of apoptosis in lung tumours across an extensive time course after *Trp53* restoration (Supplementary Fig. 6). Collectively, these data demonstrate that adenomas do not respond to p53 restoration, whereas adenocarcinomas are sensitive. Moreover, *Trp53* mutation *per se* does not induce phenotypic changes in tumour grade but rather creates a permissive environment for the outgrowth of cells that have undergone additional steps in tumour progression. Finally, the alterations that drive tumour progression can also stimulate p53-dependent cellular responses.

To interrogate the mechanisms that drive tumour progression, we performed immunohistochemistry on tumours from $Kras^{LA2/+};Trp53^{+/+}$ and $Kras^{LA2/+};Trp53^{LSL/LSL}$ animals to assess the activity of multiple relevant pathways during the adenoma-adenocarcinoma transition. We found that phosphorylation levels of Mek1/2 (p-Mek, also known as Map2k1/2) and p42/p44 MAPK (p-Erk, also known as Mapk1) was markedly higher in adenocarcinomas compared to adenomas (Fig. 3a, b). This observation indicated that amplified MAPK signalling could drive progression of $Kras^{G12D}$-initiated lung cancer. High levels of MAPK signalling downstream of oncogenic *Kras* induces cell cycle arrest/senescence mediated by Arf (a product of the *Cdkn2a* locus) and p53 in multiple cell types *in vitro*[7–9]. In contrast, physiological levels of oncogenic signalling elicited by a single oncogenic *Kras* allele do not activate the Arf/p53 tumour suppressor pathway and instead can drive proliferation and tumorigenesis in many cell types[10–14]. Some cancer models show that mutation of *Ras* family members can initiate tumorigenesis, while amplification of oncogenic *Ras* or loss of the wild-type *Ras* allele is associated with tumour progression[15–17]. Thus, we proposed that amplification of oncogenic signalling could simultaneously drive tumour progression and the outgrowth of cells that had inactivated the p53 pathway during the natural course of tumour evolution. Consistent with this hypothesis, fluorescent *in situ* hybridization (FISH) analysis showed that a subset of adenocarcinomas with high p-Erk had copy number gains of the *Kras* locus. Conversely, copy number alterations of *Kras* were never seen in adenomas (Fig. 3c). Together, these observations indicate that although the mechanisms that amplify oncogenic signalling are likely to be diverse, MAPK signal amplification typifies $Kras^{LA2}$ lung adenocarcinomas and may drive progression towards malignancy.

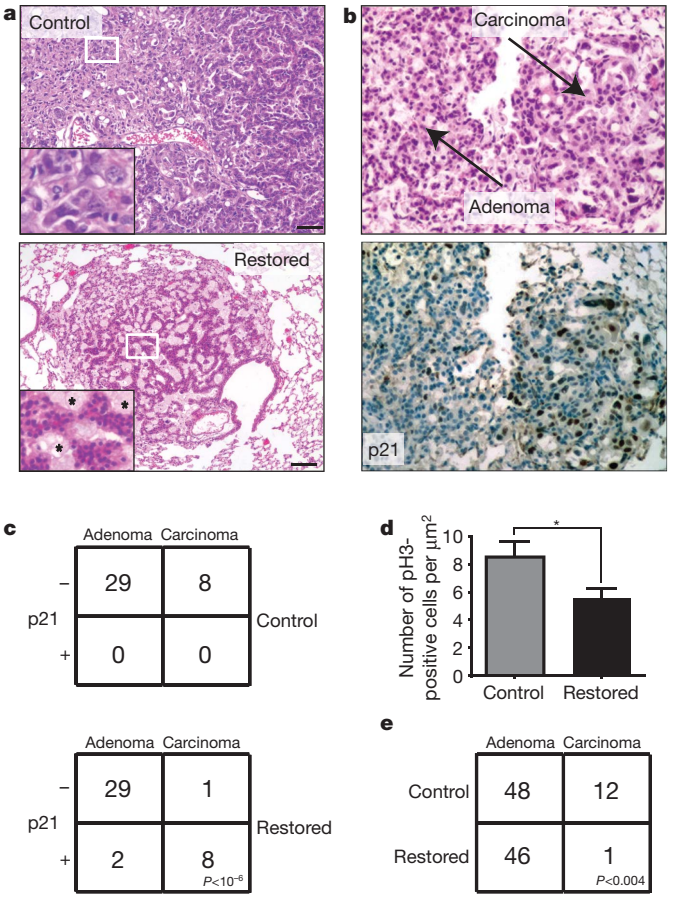

Figure 2 | Adenocarcinoma cells are sensitive to *Trp53* restoration and are specifically eliminated from lung tumours. **a**, Histological sections from control and *Trp53*-restored tumours stained with haematoxylin and eosin. Inset of *Trp53*-restored tumours show monomorphic nuclei and tumour fissures filled with foam macrophages (asterisks). Scale bars, 50 μm. **b**, Tumour sections 3 days after *Trp53* restoration. Haematoxylin and eosin-stained tumour section (top) with adenoma and carcinoma areas indicated. Serial section stained with p21 antibody (bottom). **c**, Contingency tables showing coincidence of p21 and adenocarcinoma 3 days after *Trp53* restoration. **d**, Number of pH3-positive cells per μm^2 for each tumour. Average and s.d. are shown. *Trp53* restoration leads to significantly fewer mitoses. $*P < 0.05$ **e**, Tumour grades in control and *Trp53* restored animals two weeks after initial treatment (vehicle-treated tumours, $n = 60$; tamoxifen-treated tumours, $n = 47$).

To test whether cells with amplified MAPK signalling persist after *Trp53* restoration, we analysed $Kras^{LA2/+};Trp53^{LSL/LSL};Rosa26^{CreERT2}$ animals across a time course after tamoxifen administration. Loss of high p-Erk staining cells was evident 1 week after *Trp53* restoration (Supplementary Fig. 7). Compared to controls, tumours with *Trp53* restored showed significantly fewer p-Erk positive tumours after 2 weeks (Fig. 3d). This observation, in conjunction with the selective loss of histologically advanced tumour cells seen after *Trp53* restoration, suggests that amplified MAPK signalling is incompatible with p53 expression.

Next, we micro-dissected tumours from $Kras^{LA2/+};Trp53^{LSL/LSL}$ mice and performed gene expression analysis to characterize better the molecular alterations that drive tumour progression. We developed an 'adenocarcinoma signature' by comparing the gene expression profiles of adenocarcinomas and adenomas (Fig. 4a). Gene set enrichment analysis showed that pathways associated with increased proliferation such as cell cycle processes, the Ras pathway and c-myc (also known as Myc) target genes were enriched in adenocarcinomas compared to adenomas (Fig. 4b). Other gene sets associated with adenocarcinomas were chemokine regulation, inflammation and immune responses, as

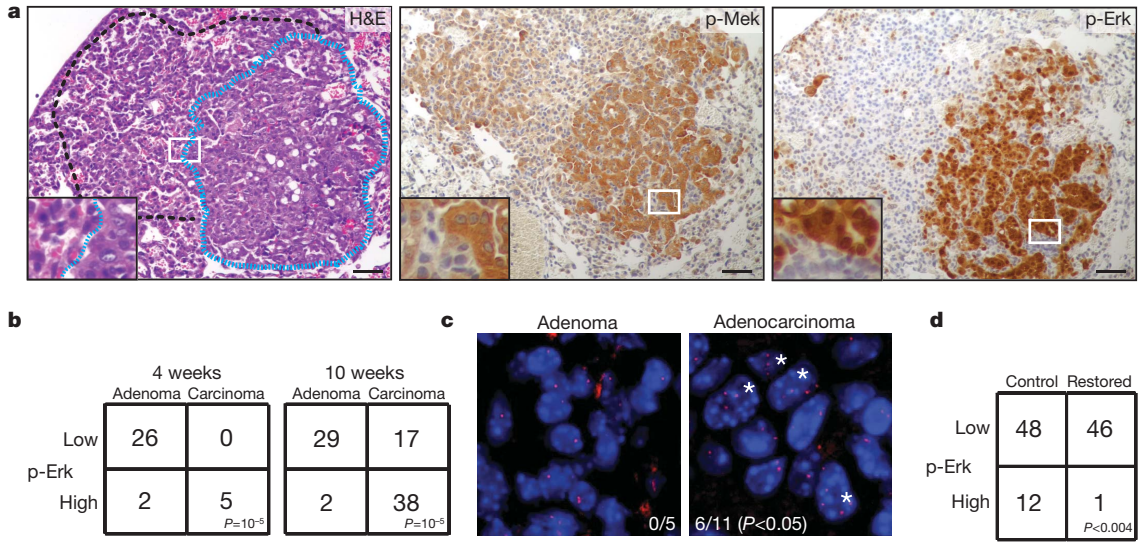

Figure 3 | Adenocarcinomas are typified by amplified MAPK signalling. **a**, Serial tumour sections of a mixed grade tumour stained with haematoxylin and eosin (H&E), anti-p-Mek or anti-p-Erk. Dashed lines outline high-grade (blue) and low-grade (black) areas. **b**, Contingency tables representing number of tumours with high or low MAPK signalling, and the corresponding tumour grades in $Kras^{LA2/+};Trp53^{LSL/LSL}$ at the 4- and 10-week time points. **c**, A subset of tissue sections from **a** were stained with bacterial artificial chromosome probes surrounding the *Kras* locus on mouse chromosome 6. *Kras* signals (red) and DAPI/DNA (blue) counter stain are shown in an adenoma and a carcinoma. Asterisks indicate nuclei with greater than two Kras signals. **d**, Contingency plot of tumours with high p-Erk staining shows significantly fewer tumours with high p-Erk staining after *Trp53* restoration.

well as *AP1* and *PEA3* (also known as *Jun* and *Etv4*, respectively) target genes. These data indicate that multiple pathways are enhanced upon progression to malignancy coincident with, or as a result of, amplified MAPK signalling.

To assess the response to p53 restoration in adenocarcinomas at the level of gene expression, we profiled micro-dissected tumours from $Kras^{LA2/+};Trp53^{LSL/LSL};Rosa26^{CreERT2}$ mice seven days after *Trp53* restoration. Each tumour was histologically analysed for evidence consistent with a p53 response and the appearance of some adenocarcinoma features (Supplementary Fig. 7). We used the adenocarcinoma signature to perform hierarchical clustering on these p53-restored samples together with adenomas and adenocarcinomas. Interestingly, the p53-restored samples clustered with adenomas with high confidence. Additionally, adenocarcinoma specific gene sets were de-enriched in *Trp53*-restored tumours (Fig. 4a, b). These data are consistent with our observation that adenocarcinoma cells are specifically culled from these tumours leaving behind adenoma cells that are unresponsive to p53 restoration.

Hyperactive MAPK signalling has been shown to induce the transcription of *Cdkn2a*, leading to expression of Arf, an upstream activator of p53 (ref. 9). Consistent with this mechanism of triggering the p53 pathway, we found that *Cdkn2a* expression was higher in adenocarcinomas compared to adenomas (Supplementary Fig. 8a). Moreover, in tumours from $Kras^{LA2/+};Trp53^{LSL/LSL}$ mice, p-Erk co-localizes with Arf staining by immunofluorescence and immunohistochemistry specifically in adenocarcinomas and the higher-grade areas of mixed-grade tumours (Fig. 4c and Supplementary Fig. 8b, c). To test the functional requirement of Arf in the p53 response, we studied cell lines generated from $Kras^{LA2/+};Trp53^{LSL/LSL};Rosa26^{CreERT2}$ lung adenocarcinomas. As we had observed *in vivo*, restoration of *Trp53* in cell culture led to prolonged cell cycle arrest without appreciable cell death. Further, the gene expression program elicited by *Trp53* restoration in these cell lines is similar to that observed *in vivo*, validating them as a relevant model with which to test Arf dependency for activation of p53 responses after *Trp53* restoration (Supplementary Fig. 9). We expressed shRNAs (short hairpin RNAs) targeted against either an Arf-specific

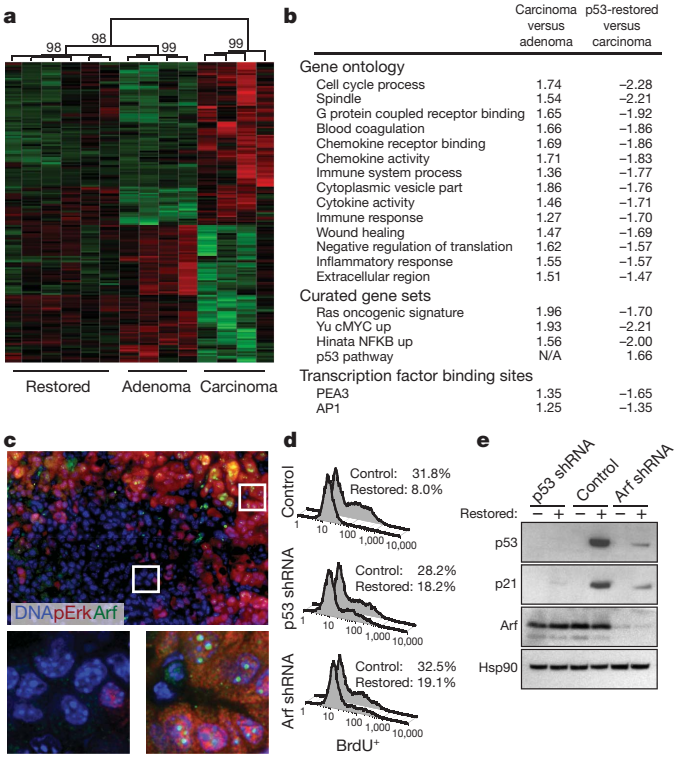

Figure 4 | Arf is specifically expressed in adenocarcinomas and sensitizes lung cancer cells to *Trp53* restoration. **a**, Hierarchical clustering of samples based on the adenocarcinoma signature. Confidence values (percent) are indicated at the top of major clades. **b**, GSEA (gene set enrichment analysis). Notable gene sets are listed with normalized enrichment scores for each comparison. Positive and negative enrichment scores indicate correlation and anti-correlation, respectively. **c**, Tissue sections from $Kras^{LA2/+};Trp53^{LSL/LSL}$ adenomas, mixed-grade tumours, and adenocarcinomas were co-labelled with antibodies to p-Erk (red) and Arf (green). Six adjacent fields of view of a mixed-grade tumour (top), and deconvoluted *z*-stack images (bottom) of dashed regions of an adenoma area (left) and adenocarcinoma area (right) are shown. **d**, Proliferation assay in adenocarcinoma-derived cell lines. Knockdown with retrovirally expressed shRNAs to *Trp53* or *Cdkn2a* (Arf-specific transcript), or control cells 48 h after *Trp53* restoration. Percentage of $BrdU^+$ cells is indicated. **e**, Adenocarcinoma cell lysates from **d** were subjected to immunoblot analysis for p53, p21, Arf and Hsp90 (loading control).

transcript of *Cdkn2a* or *Trp53* in cell lines before *Trp53* restoration. As shown in Fig. 4d, inhibition of Arf or p53 allowed cells to continue to proliferate following addition of tamoxifen. Furthermore, Arf knockdown kept p53 levels low after *Trp53* restoration and limited the induction of the p53 target gene p21 (Fig. 4e and Supplementary Fig. 9c). These data indicate that Arf is required for p53 restoration-induced cell cycle arrest in this system.

Our failure to detect apoptosis following *Trp53* restoration stands in contrast to a report published together with ours in this issue[18]. The most likely explanation for this discrepancy is the different technologies used to control p53 function. Whereas our method restores a disrupted gene back to its wild-type state and allows otherwise normal p53 expression, our colleagues used a p53-ER fusion protein that might be expected to accumulate to high levels in advanced tumours that express Arf[18]. Thus, in that setting, p53-ER may induce more robust responses that include apoptosis when activated by tamoxifen.

Given our results on the requirement of Arf in the p53 response in this setting, one might imagine that Arf and p53 mutations would have equivalent effects in lung cancer progression. However, unlike in $Kras^{LA2/+};Trp53^{LSL/LSL}$ mice, carcinomas rarely develop in $Kras^{LA2}$ mice carrying Arf mutations[19]. Thus, the clear effects of p53 mutation on tumour progression are likely to reflect additional functions of p53, including its role in responding to DNA damage and other forms of genomic instability[20].

The possibility that reactivation of defective p53 pathways will lead to variable and incomplete tumour regression is intriguing and may have important implications for anti-cancer therapies. As a tumour naturally progresses, multiple related, but genetically distinct clones co-evolve within the tumour. Conceptually akin to resistance mutations that are selected after targeted cancer therapies, pharmacological targeting of mutations that drive tumour progression, rather than initiation, may lead to significant pruning of some clones but leave behind others that still have significant potential to progress further in tumorigenesis. Although it is generally accepted that the elimination of the most advanced tumour cells within a cancer will be a significant benefit in cancer therapy, strategies to eliminate, or prevent progression of, the less advanced residual tumour cells may be important to allow durable therapeutic responses.

METHODS SUMMARY

Mice. Animal studies were approved by the Committee for Animal Care, and conducted in compliance with the Animal Welfare Act Regulations and other federal statutes relating to animals and experiments involving animals and adheres to the principles set forth in the Guide for the Care and Use of Laboratory Animals, National Research Council, 1996 (institutional animal welfare assurance no. A-3125–01). All animals were maintained on a mixed C57BL/6J x 129SvJ strain. Tamoxifen (Sigma) was administered intraperitoneally twice weekly at 200 μg per gram total body weight. Micro-computed tomography analysis was performed as described[21].

Histology and immunohistochemistry. Formalin-fixed paraffin-embedded sections were stained with antibodies against p53 (Novocastra NCL-p53-CM5p), phosphorylated Mek1/2 (p-Mek), phosphorylated p42/p44 MAPK (p-Erk), cleaved caspase 3 (CC3), phosphorylated histone H3 (pH3) (Cell Signaling Technology), p19/Arf, or p21 (F5) (Santa Cruz Biotech). Immunofluorescence images were produced with a Delta Vision deconvolution microscope (Applied Precision) and SoftWorx software. Terminal deoxynucleotidyl transferase dUTP nick-end labelling (TUNEL) staining was performed following the manufacturer's instructions (*In situ* Cell Death Detection kit, Roche). FISH was performed with Texas Red-labelled bacterial artificial chromosome (BAC) clone RP23-188E5.

Gene expression analysis. RNA was extracted from micro-dissected tumours using TRIzol (Invitrogen). RNA was processed, labelled and hybridized to Affymetrix 430A_v2 chips. Gene expression data was deposited in Gene Expression Omnibus (GSE23875).

Cell lines. Cell lines were derived from $Kras^{LA2/+};Trp53^{LSL/LSL};Rosa26^{CreERT2}$ adenocarcinomas. Retroviruses expressing shRNAs were designed and cloned as described previously[22]. Cell cycle analysis was performed according to the APC BrdU Flow Kit (BD Parmingen).

Immunoblot analysis. p53 protein was detected using NCL-p53-505 (Novocastra), Hsp90 served as a loading control and was detected using a monoclonal antibody (BD Transduction Laboratories). Other antibodies were as for immunohistochemistry.

Full Methods and any associated references are available in the online version of the paper at www.nature.com/nature.

Received 22 December 2009; accepted 27 September 2010.

1. Hanahan, D. & Weinberg, R. A. The hallmarks of cancer. *Cell* **100,** 57–70 (2000).
2. Selivanova, G. & Wiman, K. G. Reactivation of mutant p53: molecular mechanisms and therapeutic potential. *Oncogene* **26,** 2243–2254 (2007).
3. Wang, W. & El-Deiry, W. S. Restoration of p53 to limit tumor growth. *Curr. Opin. Oncol.* **20,** 90–96 (2008).
4. Xue, W. *et al.* Senescence and tumour clearance is triggered by p53 restoration in murine liver carcinomas. *Nature* **445,** 656–660 (2007).
5. Martins, C. P., Brown-Swigart, L. & Evan, G. I. Modeling the therapeutic efficacy of p53 restoration in tumors. *Cell* **127,** 1323–1334 (2006).
6. Ventura, A. *et al.* Restoration of p53 function leads to tumour regression *in vivo*. *Nature* **445,** 661–665 (2007).
7. Serrano, M., Lin, A. W., McCurrach, M. E., Beach, D. & Lowe, S. W. Oncogenic *ras* provokes premature cell senescence associated with accumulation of p53 and $p16^{INK4a}$. *Cell* **88,** 593–602 (1997).
8. Palmero, I., Pantoja, C. & Serrano, M. $p19^{ARF}$ links the tumour suppressor p53 to Ras. *Nature* **395,** 125–126 (1998).
9. Lin, A. W. *et al.* Premature senescence involving p53 and p16 is activated in response to constitutive MEK/MAPK mitogenic signaling. *Genes Dev.* **12,** 3008–3019 (1998).
10. Tuveson, D. A. *et al.* Endogenous oncogenic $K\text{-}ras^{G12D}$ stimulates proliferation and widespread neoplastic and developmental defects. *Cancer Cell* **5,** 375–387 (2004).
11. Haigis, K. M. *et al.* Differential effects of oncogenic K-Ras and N-Ras on proliferation, differentiation and tumor progression in the colon. *Nature Genet.* **40,** 600–608 (2008).
12. Sarkisian, C. J. *et al.* Dose-dependent oncogene-induced senescence *in vivo* and its evasion during mammary tumorigenesis. *Nature Cell Biol.* **9,** 493–505 (2007).
13. Jackson, E. L. *et al.* Analysis of lung tumor initiation and progression using conditional expression of oncogenic *K-ras*. *Genes Dev.* **15,** 3243–3248 (2001).
14. Johnson, L. *et al.* Somatic activation of the *K-ras* oncogene causes early onset lung cancer in mice. *Nature* **410,** 1111–1116 (2001).
15. Quintanilla, M., Brown, K., Ramsden, M. & Balmain, A. Carcinogen-specific mutation and amplification of Ha-*ras* during mouse skin carcinogenesis. *Nature* **322,** 78–80 (1986).
16. Bremner, R. & Balmain, A. Genetic changes in skin tumor progression: correlation between presence of a mutant *ras* gene and loss of heterozygosity on mouse chromosome 7. *Cell* **61,** 407–417 (1990).
17. Liu, M. L. *et al.* Amplification of Ki-*ras* and elevation of MAP kinase activity during mammary tumor progression in C3(1)/SV40 Tag transgenic mice. *Oncogene* **17,** 2403–2411 (1998).
18. Junttila, M. R. *et al.* Selective activation of p53-mediated tumour suppression in high-grade tumours *Nature* doi:10.1038/nature09526 (this issue).
19. Young, N. P. & Jacks, T. Tissue-specific $p19^{Arf}$ regulation dictates the response to oncogenic K-ras. *Proc. Natl Acad. Sci. USA* **107,** 10184–10189 (2010).
20. Lane, D. P. p53, guardian of the genome. *Nature* **358,** 15–16 (1992).
21. Meylan, E. *et al.* Requirement for NF-κB signalling in a mouse model of lung adenocarcinoma. *Nature* **462,** 104–107 (2009).
22. Dickins, R. A. *et al.* Probing tumor phenotypes using stable and regulated synthetic microRNA precursors. *Nature Genet.* **37,** 1289–1295 (2005).

Supplementary Information is linked to the online version of the paper at www.nature.com/nature.

Acknowledgements We would like to thank M. DuPage and C. Kim for critical reading of the manuscript. We are indebted to D. Crowley, E. Vasile and M. Griffin at the Koch Institute Core facilities (supported by Cancer Center Support (core) grant P30-CA14051 from the National Cancer Institute). We are grateful to M. Luo for microarray support. We thank M. Leversha at MSKCC for FISH. D.M.F. has been supported by the American Cancer Society (New England Area Fellow), and is a current Fellow of the Leukemia and Lymphoma Society. K.K.K. is supported by the John Reed Fund of the MIT undergraduate research program. M.M.W. was a Merck Fellow of the Damon Runyon Cancer Research Foundation and a Genentech postdoctoral fellow. T.J. is the David H. Koch Professor of Biology and a Daniel K. Ludwig Scholar. The Howard Hughes Medical Institute supported this work.

Author Contributions D.M.F. and T.J. conceived of the experiments and wrote the manuscript with comments from all authors; D.M.F., K.K.K, C.C., S.E.T. and R.R. performed the experiments and analysed the data; M.M.W. and F.J.S.-R. gave conceptual advice; R.B. performed histological evaluations; C.A.W. performed bioinformatics data analysis; and M.T.H. provided reagents and conceptual advice.

Author Information Gene expression data was deposited in Gene Expression Omnibus (GSE23875). Reprints and permissions information is available at www.nature.com/reprints. The authors declare no competing financial interests. Readers are welcome to comment on the online version of this article at www.nature.com/nature. Correspondence and requests for materials should be addressed to T.J. (tjacks@mit.edu).

METHODS

Mice. Animal studies were approved by the Committee for Animal Care, and conducted in compliance with the Animal Welfare Act Regulations and other federal statutes relating to animals and experiments involving animals and adheres to the principles set forth in the Guide for the Care and Use of Laboratory Animals, National Research Council, 1996 (institutional animal welfare assurance no. A-3125–01). All animals were maintained on a mixed C57BL/6J x 129SvJ strain. *Kras*^{LA2}, *Trp53*^{LSL} and *Rosa26*^{CreERT2} mice have been described[6,14]. Tamoxifen (Sigma) was dissolved in corn oil (Sigma) and administered intraperitoneally twice weekly at 200 μg per gram total body weight. Lung tumour volumes were acquired from isoflurane-anesthetized mice using eXplore Locus MicroCT imager. Image acquisition was performed using eXplore Scan Control software, using a 45-μm voxel size program, and three-dimensional reconstruction was performed using eXplore Reconstruction Utility software. High-resolution tomograms were generated and individual tumour volumes were measured and calculated using MicroView software (all from GE Healthcare). For serial micro-computed tomography analysis, the relative size of each tumour was compared to the tumour volume at the 10-week time point.

Statistics. *P*-values indicated in contingency tables and FISH analysis were established by Fisher's exact test. Significance values from tumour volume studies and, proliferation (pH3) analyses were evaluated by Student's two-tailed *t*-test. Microarray statistics are described below.

Histology. All tissues were fixed in 10% formalin overnight, transferred to 70% ethanol, then embedded in paraffin. Four-micrometre sections were cut.

Tumour grading. All histological analyses were assisted by a board certified veterinary pathologist (R.B.). A tumour was scored positive for pleomorphic nuclei if it contained three or more such cells.

Immunohistochemistry. Slides were stained with haematoxylin and eosin or with antibodies to p53 (Novocastra NCL-p53-CM5p), phosphorylated Mek1/2 (p-Mek), phosphorylated p42/p44 MAPK (p-Erk), cleaved caspase 3 (CC3), phosphorylated histone H3 (pH3) (Cell Signaling Technology), p19/Arf, or p21 (F5) (Santa Cruz Biotech). Antigen retrieval was performed in 10 mM sodium citrate pH 6.0 by heating in a pressure cooker for 10 min.

Immunofluorescence. Images were captured with a 60×, 1.3 NA objective on a Delta Vision deconvolution microscope (Applied Precision). Image *z*-stacks were deconvoluted with SoftWorx software package, and maximum projections saved as tiff files. TUNEL staining was performed following the manufacturer's instructions (*In situ* Cell Death Kit, Roche).

FISH. BAC clone RP23-188E5 was labelled with Texas Red dye. Hybridizations and probe labelling was performed at the Memorial Sloan Kettering Cancer Center, cytogenetics core facility.

Cell line derivation, retrovirus production, and shRNA cloning. Tumours were isolated from *Kras*$^{LA2/+}$;*Trp53*$^{LSL/LSL}$;*Rosa26*^{CreERT2} animals, dissociated with collagenase and trypsin for one hour at 37 °C, and then grown in Dulbecco's modified Eagle media plus 10% fetal bovine serum. Retroviruses were produced by transfection of Phoenix cells (Lipofectamine 2000) and shRNAs were designed and cloned as previously described[22]. The 97-nucleotide oligomer used to generate the shRNA targeting the *Cdkn2a* locus was: 5′-TGCTGTTGACAGTGAGCGACGCTCTGGCTTTCGTGAACATTAGTGAAGCCACAGATGTAATGTTCACGAAAGCCAGAGCGCTGCCTACTGCCTCGGA-3′. Cell cycle analysis was performed according to the APC BrdU Flow Kit (BD Parmingen). Data are representative of five cell lines derived from independent tumours. Cell lysates were prepared with RIPA buffer before separation on 4–12% BisTRIS NuPAGE gels (Invitrogen). Mouse p53 protein was detected using NCL-p53-505 (Novocastra). Hsp90 served as a loading control and was detected using a monoclonal antibody (BD Transduction Laboratories). Other antibodies were as for immunohistochemistry. Data are representative of two independent cell lines sorted by green fluorescent protein expression (expressed from within the shRNA retrovirus[22]) for purity.

Gene expression analysis. Microarray analysis. RNA was extracted from microdissected adenocarcinomas, adenomas and *Trp53*-restored tumours from *Kras*$^{LA2/+}$;*Trp53*$^{LSL/LSL}$ mice using TRIzol (Invitrogen). RNA was processed, labelled and hybridized to Affymetrix 430A_v2 chips according to the manufacturer's instructions. Affymetrix data analysis was done using statistical tools provided by the R and Bioconductor projects (http://cran.r-project.org/; http://www.bioconductor.org/). Data import and quality control assessment was done using the packages Affy and AffyPLM[23]. Data was summarized and normalized using gcRMA[24]. Differential expression analysis was carried out using limma[25]. All the R commands, input data and environment-specific details required to duplicate these analyses are located here:
http://luria.mit.edu/caw_web/Feldser_supplemental/EtOH_TAM/
http://luria.mit.edu/caw_web/Feldser_supplemental/tumours/

Hierarchical clustering with *P*-values. The 'adenocarcinoma signature' consists of 71 genes up-regulated in adenocarcinomas and 57 genes up-regulated in adenomas ($P < 0.05$ and fold change > 1.75). Expression values were row-normalized using *z*-scores and the resulting data were subjected to hierarchical clustering (Ward's method) and a sample dendrogram was produced using the R package pvclust[26]. The heat map was generated using Spotfire DecisionSite 9.1.1. The required R commands and the input data are located here:
http://luria.mit.edu/caw_web/Feldser_supplemental/pvclust/

Gene set enrichment analysis (GSEA). GSEA (http://www.broad.mit.edu/gsea/) was used to examine the distribution of the curated gene sets from the Broad Institute's MsigDB (http://www.broadinstitute.org/gsea/msigdb/index.jsp) in lists of genes ordered according to differential expression between various conditions. Positive and negative enrichment scores indicate correlation and anti-correlation respectively. The resulting data and the files required to duplicate these analyses are available here:
http://luria.mit.edu/caw_web/Feldser_supplemental/EtOH_TAM_GSEA/
http://luria.mit.edu/caw_web/Feldser_supplemental/tumours_GSEA/

23. Bolstad, B. M., Collin, F., Simpson, K. M., Irizarry, R. A. & Speed, T. P. Experimental design and low-level analysis of microarray data. *Int. Rev. Neurobiol.* **60,** 25–58 (2004).
24. Bolstad, B. M., Irizarry, R. A., Gautier, L. & Wu, Z. in *Bioinformatics and Computational Biology Solutions using R and Bioconductor* (eds Gentleman, R., Carey, V., Huber, W., Irizarry, R. & Dudoit, S.) Ch. 2, 13–32 (Springer, 2005).
25. Smyth, G. K., Michaud, J. & Scott, H. S. Use of within-array replicate spots for assessing differential expression in microarray experiments. *Bioinformatics* **21,** 2067–2075 (2005).
26. Suzuki, R. & Shimodaira, H. Pvclust: an R package for assessing the uncertainty in hierarchical clustering. *Bioinformatics* **22,** 1540–1542 (2006).